Efficient solution-processed infrared photovoltaic cells: Planarized all-inorganic bulk heterojunction devices via inter-quantum-dot bridging during growth from solution

Ethan J. D. Klem, Dean D. MacNeil, Paul W. Cyr, Larissa Levina, and Edward H. Sargent[a)]
Department of Electrical and Computer Engineering, University of Toronto, Toronto, Ontario M5S 3G4, Canada

(Received 13 March 2007; accepted 6 April 2007; published online 2 May 2007)

Solution-processed thin-film organic, inorganic, and hybrid photovoltaic devices have achieved power conversion efficiencies as high as 5%. However, these devices remain limited by their capture of visible energy; more than a half of the sun's power lies in the infrared. Herein the authors demonstrate photovoltaic devices effective across the visible and all the way out to 1700 nm. Only through the use of ethanedithiol as a bridging molecule to affect interparticle linking were they able to achieve fabrication of smooth, continuous quantum dot films on rough, high-surface area transparent metal oxides. This allowed them to increase light absorption while maintaining efficient charge separation and extraction and at the same time avoiding electrical short circuits. They obtained monochromatic infrared power conversion efficiencies of 1.3%, a 50-fold gain over the previous published record of 0.025% in IR solution-processed photovoltaics. The authors demonstrate quantum size-effect tuning of device band gaps relevant to multijunction solar cells. © *2007 American Institute of Physics*. [DOI: 10.1063/1.2735674]

Low-cost, large-area solar cells offer the prospect of economically sustainable clean energy capture. The best solid-state solution-processed solar cells have to date produced power conversion efficiencies in the range of 3%–5%.[1,2] One factor limiting their further improvement is solution-processed photovoltaics' transparency to the sun's infrared rays. Half of the sun's power reaching the earth lies beyond 700 nm, and one third beyond 1000 nm. However, the best reported inorganic thin-film nanocrystal-based devices absorb only to the blue of 800 nm,[1] and organic polymer/C_{70}-derivative devices are effective out to about 1000 nm,[3] with their peak efficiency lying at 800 nm.

For these reasons, there exists an urgent need to realize solution-processed short-wavelength infrared (SWIR) photovoltaic devices. In 2005 it was reported that spin-coated colloidal quantum dots, combined with a polymer matrix, produced a photovoltaic effect.[4] However, these blend devices exhibited external quantum efficiencies less than 0.006% at 975 nm. Further development of bilayer devices has so far improved external quantum efficiencies to 0.4% at 975 nm.[5]

Here we report a nearly two-order-of-magnitude increase in the external quantum efficiency of solution-processed SWIR photovoltaics relative to previous reports. Our approach was informed by two recent findings in the electronic properties of solution-processed quantum dot films. First, it was recently shown that films of pure quantum dots—with no heterostructure matrix and with insulating organic ligands modified or removed—can exhibit mobilities above 0.1 $cm^2/V\,s$.[6,7] Second, since the previous record exhibited transport-limited external quantum efficiencies,[5] it was evident that a rough-interface architecture that increased absorbance while keeping exciton-separation efficiency high would be required.

We used as a bottom (nonoptically absorbing) electron-accepting electrode high-surface-area nanoparticular indium tin oxide (ITO). Solution-processable high-surface-area materials capable of forming a type-II heterojunction suitable for charge separation include ZnO, SnO_2, and ITO.[8–10] The inset of Fig. 4 shows the expected type-II energy band diagram formed between PbS and ITO. We selected this material since we were able to obtain conductivities up to five orders of magnitude higher than using ZnO or SnO_2.[11] Under photovoltaic operation, charge separation occurs at the interface between the ITO and the PbS as well as at the interface between the PbS and the Mg top contact.

We synthesized PbS nanocrystals using an organometallic route previously described.[12] As synthesized, the nanocrystals are capped with ~2.5 nm long oleic acid ligands. These impede charge transport, producing insulating thin films. To create conductive nanocrystal films, we used a solution-phase ligand exchange to replace oleate ligands with ~0.6 nm long butylamine ligands. Following ligand exchange, the butylamine-capped nanocrystals exhibited linear *IV* characteristics indicative of resistive transport.[6]

We fabricated the ITO phase of our bulk heterojunction by spin coating ITO particles, originally suspended in water, onto a glass substrate. A slurry of ITO was used that consisted of 4 g of ITO (Nanotek, Alfa Aesar) and 4 g of distilled water. To this suspension, approximately 2 ml of Triton-X surfactant (Aldrich) was added dropwise and stirred overnight, 100 μL of the slurry was then spin coated (800 rpm, 60 s) onto a 1 in. square glass slide. The slide was annealed at 310 °C for 1 h. The film was then baked in air at 310 °C for 30 min, resulting in 3 μm thick films with resistivities on the order of 0.5 Ω cm. Figures 1(a) and 1(b) show the resulting high-surface-area film.

We fabricated devices by soaking the ITO-coated substrate in a 5 mg/ml solution of butylamine-capped PbS quantum dots in chloroform for 10 min. An absorption spectrum of the device shows a nanocrystal spectral absorp-

a)Author to whom correspondence should be addressed; electronic mail: ted.sargent@utoronto.ca

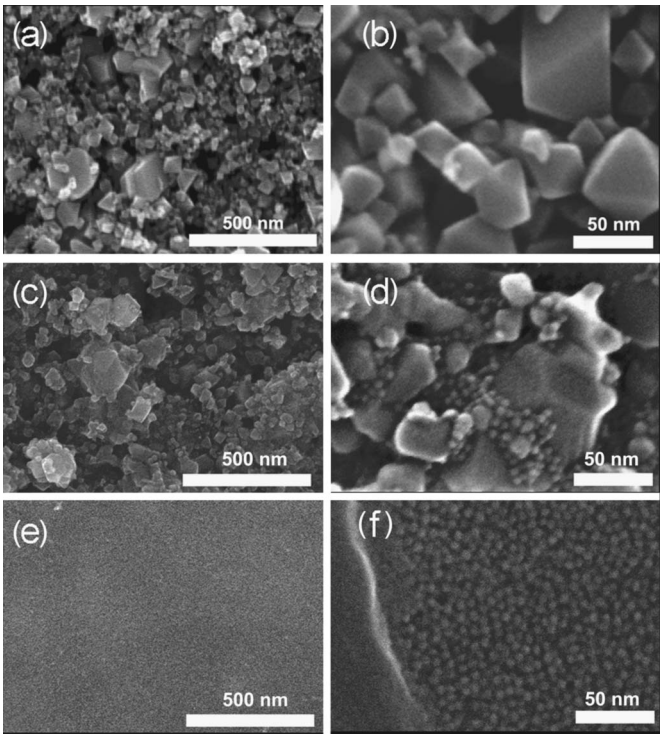

FIG. 1. SEM images of the surface of a textured ITO substrate before nanocrystal deposition and the surfaces of an ITO substrate after nanocrystal deposition with and without the use of cross-linking molecules. [(a) and (b)] Bare textured ITO substrate (c) and (d) textured ITO after nanocrystal deposition without cross-linker, showing the exposed ITO which leads to short-circuited devices. Individual nanocrystals can be seen clustered in the crevices between sintered ITO particles. [(e) and (f)] Surface of functional devices after nanocrystal deposition utilizing cross-linkers to obtain a continuous nanocrystal overcoating. The feature to the left of (f) is a portion of the nanocrystal film that is not in focus.

tion characteristic indicating that the nanocrystals have indeed deposited. Subsequent deposition iterations were employed until a saturation was observed in the growth of the nanocrystal absorption feature. Magnesium contacts (100 nm thick, 300 μm in diameter) capped by a layer of silver (100 nm thick) were then deposited via thermal evaporation; however, all of the devices fabricated using this method were found to result in short circuits when current-voltage (*IV*) curves were taken.

Figure 1(c) [taken with a Hitachi S-5200 scanning electron microscopy (SEM)] shows an area of the ITO-PbS quantum dot device before metal contacts were evaporated. The exposed bare ITO in the device led to direct contact with the deposited metal. Figure 1(d) shows a higher magnification image of the exposed bare ITO. Here individual PbS nanoparticles can be seen clustered in the crevices formed between sintered ITO particles.

We therefore sought a technique to guarantee complete coverage of the rough, spiky ITO by the PbS quantum dot layer. We expected that a linker molecule, mercaptoacetic acid, that at one end attached to the ITO via a carboxylic group, and at the other end attached to PbS via a thiol group, could lead to complete coverage. Bifunctional linker molecules of this type have been used for the attachment of monolayers of visible-sensitive quantum dots as sensitizers in metal oxide/liquid electrolyte photovoltaic cells.[13] Interestingly, we found this method, too, to lead to short circuits due to an inability of this method to create a smooth, continuous film atop the rough shards emanating from the underlying nanoporous ITO electrode.

We therefore sought not to link the PbS quantum dots directly to the ITO; but instead to link PbS nanoparticles to one another. We hoped that this would lead to lateral growth of the PbS film in such a way as to overgrow the faceted shards of ITO. This approach involved the use of a bridging molecule to facilitate interparticle linking. Although bridging molecules have been used for monolayer deposition of semiconductor nanoparticles on metal electrodes,[14] we use them instead herein to direct multilayer particle assembly in both lateral and vertical directions toward the realization of a planarized film on a rough substrate. We selected ethanedithiol for two reasons. First, thiols possess a strong affinity for Pb atoms, leading to effective competition with the existing amines for ligand-binding sites. Second, ethanedithiol is short (~0.7 nm) enough that any thiols remaining after subsequent device processing would not significantly impede charge transport. Due to dual role of our quantum dots as both light absorber and hole transport medium our use of a cross-linker molecule additionally coincided with a desire to improve electrical transport properties. Previously the charge transport mobility in thin-film transistors[7] and conducting nanoparticle solids[15] has benefited by the use of hydrazine and 1,4-pheynlenediamine as cross-linking molecules.

We fabricated devices using this cross-linker strategy by treating ITO in a 1% by volume solution of ethane-dithiol in acetonitrile for 30 min. The ITO was then soaked in a nanocrystal solution for 10 min. This procedure was repeated three times. As seen in Figs. 1(e) and 1(f), this produced smooth, continuous films. SEM images of device cross sections show that this process adds approximately 50 nm of additional thickness to the ITO film. We found that once top metal contacts had been deposited, these devices produced short-free *IV* characteristics.

We sought to demonstrate the value of quantum-size-effect tuning of quantum dot absorption onset by constructing classes of devices having two different excitonic spectral locations. We selected one nanocrystal batch with a first excitonic transition at 1340 nm; and for the longer-wavelength

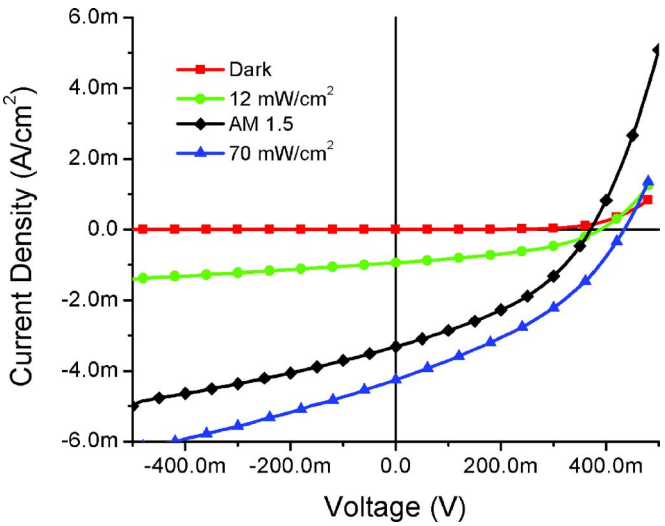

FIG. 2. (Color online) Current-voltage curves of sintered device made with nanocrystals having a first excitonic transition at 1340 nm. The AM1.5 illumination intensity was 100 mW/cm^2. Monochromatic illumination intensities of 12 and 70 mW/cm^2 were with 975 nm light.

TABLE I. Effects of sintering treatment on the performance of photovoltaic devices. All measurements performed under 12 mW/cm^2 975 nm illumination.

Device size and treatment	V_{oc} (mV)	J_{sc} (mA/cm^2)	η_P (%)	EQE (%)
1340 nm no sintering	170	0.2	0.02	2.1
1340 nm 150 °C sintering	400	1.0	1.3	10
1590 nm no sintering	70	0.02	0.003	0.2
1590 nm 130 °C sintering	85	1.5	0.3	16

device, at 1590 nm. As fabricated, devices illuminated under monochromatic of 975 nm illumination exhibited short-circuit external quantum efficiencies of 2.3% in the 1340 nm device and 0.3% in the 1590 nm nanocrystal device, in both cases with illumination intensities of 12 mW/cm^2.

We believed that thermal treatment of the devices offered the potential to improve transport within the quantum dot film, as well as charge separation across the quantum dot–ITO interface. Devices sintered in air for 3 h increased to 9% external quantum efficiency (EQE) at 975 nm (1340 nm devices) and 16% EQE (1590 nm devices). Table I summarizes the effects of sintering on the performance of the devices.

We provide current-voltage traces for the 1340 nm device in Fig. 2. We include data taken under 100 mW/cm^2 AM1.5 illumination using an Oriel solar simulator. These devices showed AM1.5 power conversion efficiencies of 0.5%. Monochromatic power conversion efficiencies at 975 nm were 1.25% for 12 mW/cm^2 illumination and 0.95% for 70 mW/cm^2 illumination. Current-voltage traces for the 1590 nm device can be seen in Fig. 3. Monochromatic power conversion efficiencies at 975 nm were 16% for 12 mW/cm^2 illumination and 5.6% for 70 mW/cm^2 illumination.

We measured the external quantum efficiency of our devices by illuminating them with monochromatic light and measuring the current generated under short-circuit photovoltaic operation. We plot in Fig. 4 the spectrally resolved external quantum efficiency which reveals a photoresponse extending to more than 1700 nm in the device fabricated

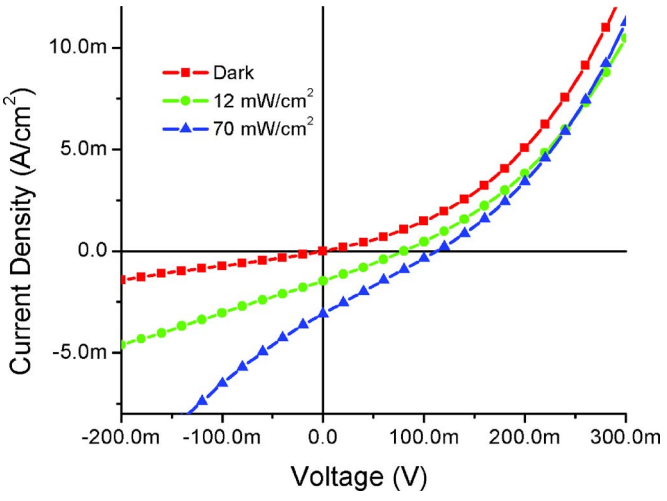

FIG. 3. (Color online) Current-voltage curves of sintered device made with nanocrystals having a first excitonic transition at 1590 nm. Monochromatic illumination intensities of 12 and 70 mW/cm^2 were with 975 nm light.

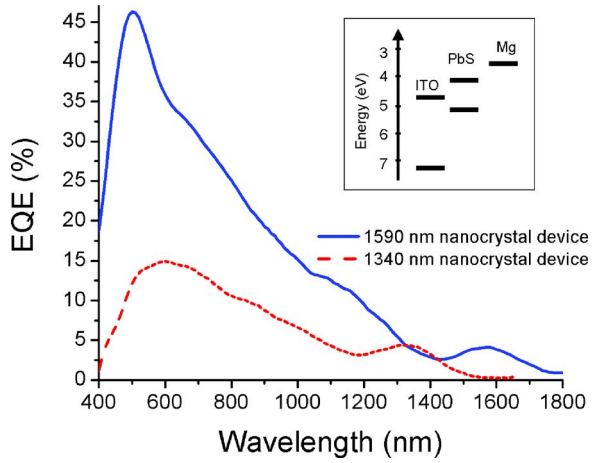

FIG. 4. (Color online) External quantum efficiency of sintered devices. The inset shows schematic of band positions of the materials used in devices. PbS conduction and valence bands are drawn for 1 eV first excitonic transition nanocrystals by employing the effective mass approximation to modify bulk energy levels.

with 1590 nm first exciton transition nanocrystals. The spectral EQE for devices composed of both sizes of nanocrystals follows closely their respective absorption spectra. A peak EQE of 46% occurred at 500 nm in the sintered 1590 nm device, while the sintered 1340 nm device exhibited a peak EQE of 15% at 590 nm. The decrease seen in EQE below about 500 nm is due primarily to increasing absorbtion in the ITO.

Devices fabricated in the manner described here were subsequently left under ambient conditions in an open circuit configuration for approximately seven months. After this time it was observed that the top deposited contacts had oxidized, significantly degrading device performance. Once a second set of contacts was deposited, however, the devices continued to function with photovoltaic efficiencies only slightly degraded from that obtained seven months earlier.

[1] I. Gur, N. A. Fromer, M. L. Geier, and A. P. Alivisatos, Science **310**, 462 (2005).
[2] W. L. Ma, C. Y. Yang, X. Gong, K. Lee, and A. J. Heeger, Adv. Funct. Mater. **15**, 1617 (2005).
[3] X. J. Wang, E. Perzon, F. Oswald, F. Langa, S. Admassie, M. R. Andersson, and O. Inganas, Adv. Funct. Mater. **15**, 1665 (2005).
[4] S. A. McDonald, G. Konstantatos, S. G. Zhang, P. W. Cyr, E. J. D. Klem, L. Levina, and E. H. Sargent, Nat. Mater. **4**, 138 (2005).
[5] A. Maria, P. W. Cyr, E. J. D. Klem, L. Levina, and E. H. Sargent, Appl. Phys. Lett. **87**, 213112 (2005).
[6] G. Konstantatos, I. Howard, A. Fischer, S. Hoogland, J. Clifford, E. Klem, L. Levina, and E. H. Sargent, Nature (London) **442**, 180 (2006).
[7] D. V. Talapin and C. B. Murray, Science **310**, 86 (2005).
[8] R. K. Swank, Phys. Rev. **153**, 844 (1967).
[9] P. V. Kamat, I. Bedja, S. Hotchandani, and L. K. Patterson, J. Phys. Chem. **100**, 4900 (1996).
[10] K. H. Lee, H. W. Jang, K. B. Kim, Y. H. Tak, and J. L. Lee, J. Appl. Phys. **95**, 586 (2004).
[11] J. Ederth, P. Johnsson, G. A. Niklasson, A. Hoel, A. Hultaker, P. Heszler, C. G. Granqvist, A. R. van Doorn, M. J. Jongerius, and D. Burgard, Phys. Rev. B **68**, 155410 (2003).
[12] M. A. Hines and G. D. Scholes, Adv. Mater. (Weinheim, Ger.) **15**, 1844 (2003).
[13] I. Robel, V. Subramanian, M. Kuno, and P. V. Kamat, J. Am. Chem. Soc. **128**, 2385 (2006).
[14] E. Granot, F. Patolsky, and I. Willner, J. Phys. Chem. B **108**, 5875 (2004).
[15] Dong Yu, Congjun Wang, and Philippe Guyot-Sionnest, Science **300**, 1277 (2003).